

PIV and aerodynamic forces analysis of a helicopter operating around a building by wind-tunnel experiments

R. Bardera¹, J.C. Matías², and E. Barroso³ National Institute for Aerospace Technology (INTA), Spain

Abstract:

Buildings in cities generate complex flows, with high velocity gradients and turbulence intensities that can make complex the helicopter landing and take-off maneuvers for pilots. Specifically, heliports at buildings are usually placed at the roof, where a big recirculation bubble is formed. Then, helicopters can be affected by the turbulent flows generated by the non-aerodynamic surfaces that compose the geometry of a building, and the aerodynamic interferences generated must be analyzed in detail.

This study analyses the interaction between the aerodynamic patterns generated by a building and those generated during the operation of the helicopter. The results are provided by a 1:170 scaled model building, and a six-component internal balance (HELIBAL) designed at INTA and integrated in a scaled helicopter model. During the wind tunnel tests, an automatic positioning system is used for placing the helicopter in different positions around the building. Particle Image Velocimetry (PIV) and smoke visualizations tests are shown to analyze the interaction between building and helicopter aerodynamics during its operation around the building, and revealed clearly interference between them. Measurements of mean forces and moments when the helicopter is hovering in multiple positions close to the building are also presented at 0.50D from the roof and 0.65D from the rear and side walls of the building. Above the roof, thrust force increases notably when the helicopter approaches the upwind corner, increasing a 57% when it is positioned towards the side corner. On the rear wall, when the helicopter is covered by the building, there are low changes on the thrust force, pitch and roll coefficients. Next to the side wall, the helicopter forces magnifies a 65% as the helicopter moves to a higher altitude, and up to 100% when it moves closer to the upwind corner.

¹ PhD aerospace engineer, Experimental Aerodynamics, <u>barderar@inta.es</u>

² PhD aerospace engineer, Experimental Aerodynamics, <u>matiasgic@inta.es</u>

³ Aerospace engineer, Experimental Aerodynamics, <u>barrosobe@inta.es</u>



1. Introduction

The most relevant capability of helicopters is to hover close to objects and structures, allowing complex emergency, police, surveillance, and transport operations in cities. However, this kind of helicopter operation can be complex for pilots who has to keep close to structures such as buildings [1], oil rigs [2], military frigates [3], or aircraft carriers [4]. This is because these non-aerodynamic structures generate flow detachments, high velocity gradients and turbulence intensities that can have a direct effect in the helicopter stability.

The specific case of aerodynamic flow around military ships is a widely analyzed topic [5-12], including different studies about the structure of the air wake generated [5, 6], numerical and experimental simulations of the wake unsteadiness [7-9], velocity data [10, 11], and turbulent flow measurements on the wake [12]. In general, they use Computational Fluid Dynamics to create models of the helicopter-ship dynamic interference [13, 14] or extract experimental data from wind tunnel, taking velocity measurements with PIV (Particle Image Velocimetry) to investigate the ship airwake and rotor downwash flow field [15-17], or using balances to measure aerodynamic forces and moments [18-22].

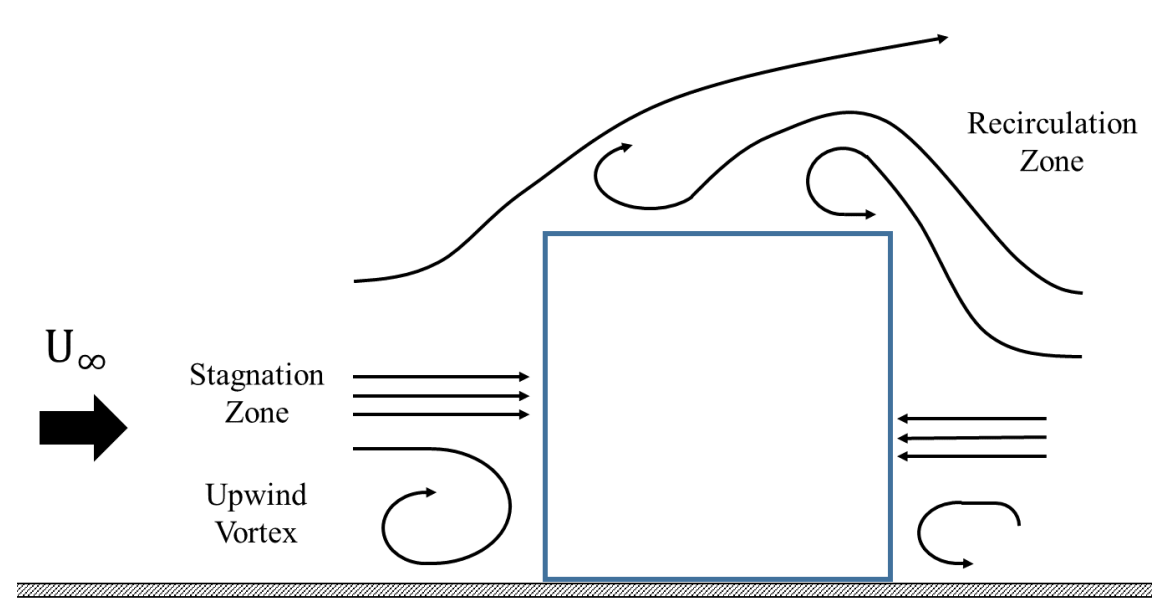


Fig. 1: Schematic representation of flow around a cube-shaped building.

Civil aerodynamics is the part of aerodynamics in charge of the study of bluff bodies with sharp edges such as buildings or bridges. These configurations present flow detachments and non-stationary aerodynamic structures. Hence, predictions are extracted by wind tunnel investigations using scaled models. Wind loads generated on building roofs and walls, or aerodynamic studies also determine the proper operation of ventilation systems, which control the building temperature and humidity [23].



A wide range of studies demonstrate that a massive flow separation with large recirculation regions is formed when the incoming flow interacts with buildings. Figure 1 shows this flow pattern around a cube-shaped building [24]. Considering a wind direction perpendicular to the upwind face, it leads to a recirculation bubble in the lower part, flow acceleration in the upper part and a stagnation point between them. Furthermore, the sharp edges cause a great detachment on the roof where low-velocity recirculation bubbles appear, affecting the operation of helicopters landing at the heliport at the roof (Figure 2).

As the flow is highly three-dimensional, when the wind incidences non-perpendicular to the wall, strong conical vortices appear on the roof [25, 26, 27] characterized by high speeds which cause large negative pressures near roof corners. And the peak of high suction generated on the roof can be estimated using a simple approximation, $c_p \sim 1/\sqrt{d}$, with d is the distance to the corner.

The combination of building and helicopter aerodynamics has gain attention in the last years as the concept of Urban Air Mobility (UAM) has received wider attention in the last years. Many companies have already developed prototypes of Personal Air Vehicles (PAV). However, the requirement of the PAV needs to be defined and some agent-based simulations have been performed to define them [28]. The definition of the requirements for the UAM infrastructure location is not an easy task. In the past, Kinley [29] studied the heliport placement in city areas leading to the conclusion that the roof of some building would be the best option and provided indications of the requirements of these buildings. However, if the urban air mobility became a more extended mean of transport, many placements for landing and taking off would be necessary. Additionally, the new concept of vehicles could need new requirements. For example, Fadhil et al. [30] propose different possible potential locations for UAM infrastructure locations: rooftops, barge over water, inside highway clover, overtop highway, overtop road, overtop rails, atop of a parking lot and atop of high-rise building.

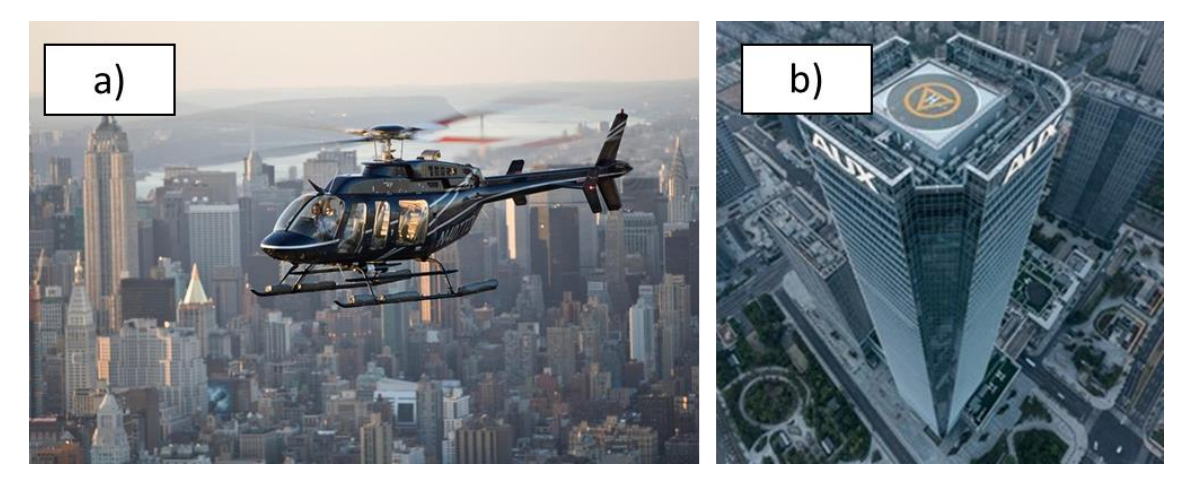


Fig. 2: a) Helicopter flying in a city. b) Heliport at the rooftop of a tower

Florence 09 - 13 September 2024



Operating helicopters inside unsteady flows requires accurate pilot corrections for controlling the aircraft, increasing its workload. Lee and Zan [15, 31] demonstrated that low frequency oscillations (0.2 to 2 Hz) are the ones that most affect the proper helicopter operation. Evaluate the effect on pilot workload can be made through the feedback from real pilots performing landing maneuvers during real situations or using high-fidelity helicopter flight simulators [32-36, 37, 38]. For example, the results contained in [33] show the influence of different motion cues, airwake conditions, and ship motion states on the pilot's overall workload.

However little information is found in the literature regarding flow around buildings and the interaction with helicopter operations. Using wind tunnel tests with scaled models of the building and helicopter equipped with an internal balance for force measurements, the main goal of this paper is to obtain aerodynamic forces and moments experienced by the helicopter during hovering on different points around the building. Different wind conditions are simulated. Standard deviations during acquisition are also registered and commented. Additionally, Particle Image Velocimetry and smoke visualizations are shown to improve understanding of the aerodynamic problem.

The structure of this paper is divided into the following sections. Section 2 will describe the experimental set-up, including the wind tunnel and Particle Image Velocimetry system used for obtaining the results. The helicopter and cube-shaped building models will be also described, including the six-component components internal balance (HELIBAL) to measure forces and moments with the helicopter, and the flow similarity between the real and scaled helicopter achieved. Section 3 will present the results of the flow visualizations around the building and aerodynamic forces and moments measured using HELIBAL on each point around the building.

2. Experimental set-up

Wind Tunnel and Particle Image Velocimetry (PIV)

The experiments were conducted in a low-speed wind tunnel at INTA, Spain (Figure 3 a). It is a closed-circuit type with an open and elliptical test section of 2 x 3 m^2 . Operating at maximum power of the engine (420 kW), the airspeed during tests can reach up to 60 m/s with turbulence intensity lower than 0.5%. At the wind tunnel test section, there is a platform that simulates the ground near the building. Streamlined leading and trailing edges were installed to minimize the interference of the platform in the flow field.

The wind tunnel is equipped with force measurements systems, and a Particle Image Velocimetry system (PIV) [39-42] for obtaining flow visualization and velocity contours around the models. For the proper working of the PIV system (figure 3 b), small tracer particles of $^{\sim}$ 1 μm in diameter are seeded in the flow and illuminated using two neodymium-doped yttrium aluminum garnet Nd:YAG pulsed lasers with a maximum energy output of 190 mJ per pulse. Synchronizing the laser pulses with the capture of



pairs of photographs, the particles positions are recorded with a digital camera and a 2048×2048 pixels Charged Coupled Device (CCD) sensor. And as the time between the first and second image of the pair is known ($\Delta t = 25~\mathrm{us}$), a cross-correlation process that uses a 2D Fast Fourier Transform (FFT) algorithm can determine the particles displacement and velocity in small interrogation windows selected of 32×32 pixels with a 50% window overlap following the Nyquist sampling criteria. During the tests, the field of view was 460 mm. All the velocity contours presented at the end of this study were obtained from a total of 100 instantaneous image pairs and represented in non-dimensional velocity contours using Tecplot360 software.

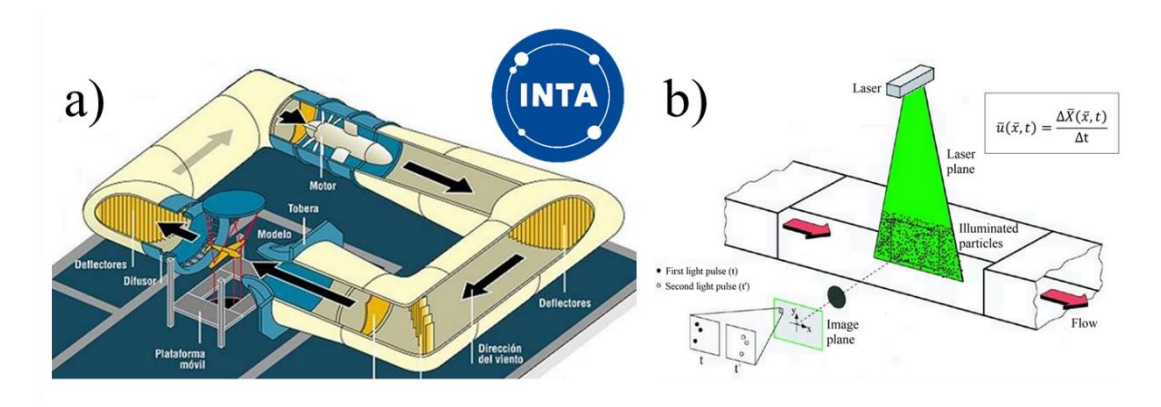


Fig. 3 a) Wind Tunnel T-1 INTA b) Scheme of Particle Image Velocimetry (PIV) system.

Building and helicopter scaled models

The building model consisted of a wooden cube of $60 \times 60 \times 60 \text{ cm}^3$. It represents a real building of 42 m in height with cube-shaped and sharp corners which could have a rooftop heliport. During wind tunnel tests the model was placed in the middle of the wind tunnel section above the platform to simulate the ground effect. The total front area of the model was on the order of 0.36m^2 , which is less than the 10% of the cross section of the wind tunnel to avoid blockage effect. The Reynolds number was 1.9×10^5 , which is above the critical Reynolds number for bluff bodies of 10^5 [43]. A photograph of the experiment is shown in Figure 4 with the scaled model of the building placed in the middle of the platform.

The helicopter model used in wind tunnel tests is also 1:70 scaled. Despite their small size, the original external geometries of the NH Industries NH-90 helicopter are accurately represented in the scaled model thanks to the 3D printing manufacturing. The helicopter has an internal balance (HELIBAL) and the full assembly is fixed to an automatic positioning system.

Then, force and moment measurements are obtained using HELIBAL, a six-component internal balance designed at INTA. It measures 3 aerodynamic forces (F_z - thrust, F_y - lateral, and F_x drag) and 3 moments (M_x - roll, M_y - pitch, and M_z - yaw). Its structure is



made of aluminum and strain gauges connected in 7 Wheatstone bridges measure deformations, which are translated to force values by a calibration matrix.

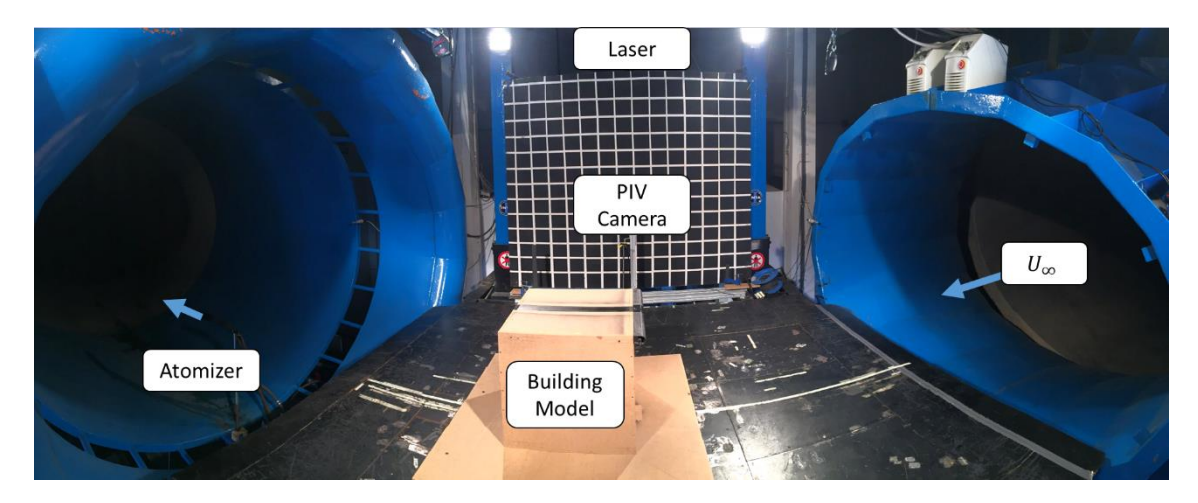


Figure 4. Building model placed at the wind-tunnel test section.

The 3D scheme displayed in Figure 5 shows the different components of the helicopter scaled model. The HELIBAL is inside a frame that fix the engine and the helicopter fuselage. The Axi 2204/54 brushless motor moves the five blades helicopter rotor of $D=230~\mathrm{mm}$ of diameter. Finally, the steel sting bar holds the full scaled helicopter assembly during the wind tunnel tests.

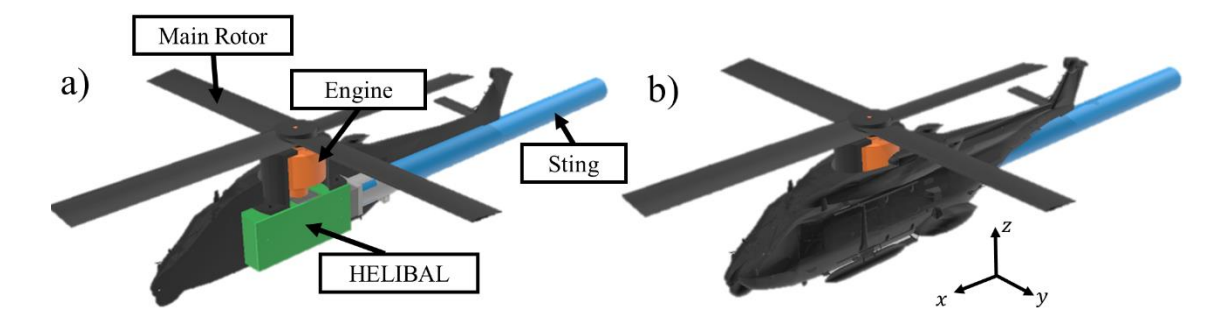


Fig. 5 Full assembly of the helicopter model.

To ensure the validity of the tests using the described helicopter assembly, it is necessary to ensure the main rotor flow similarity. This similarity can be guaranteed when the values of thrust coefficient (C_T) and advance ratio (J) of the real helicopter are achieved for the scaled model. The full-scale helicopter has a thrust coefficient during hovering flight of,

$$C_T = \frac{T_{io}}{\frac{1}{2}\rho(\Omega R)^2 S} = 9.24 \times 10^{-3}$$
 (1)

where $M=7900~{\rm kg}~{\rm kg}$, $T_{io}=W=(M\times g)~N$, $\rho=1.225~kg/m^3$, $\Omega=300~{\rm rpm}$, $R=8.15~{\rm m}$, $S=208.7~{\rm m}^2$, and $g=9.81~m/s^2$.



The same value of thrust coefficient was obtained for the model operating at 25 W (10 V and 2.5 A), resulting in a scaled rotor speed of $\Omega_s=4,350~\mathrm{rpm}$ and a similar thrust coefficient of the model of $C_T=9.24\times10^{-3}$ measured with HELIBAL.

The similarity of the advance ratio is also achieved. The wind condition represented is $U_{\infty}=20~\text{m/s}$. As the angular velocities of the real and scaled helicopter are known ($\Omega=300~\text{rpm},~\Omega_s=4,350~\text{rpm}$, and the rotor radius are R=8.15~m, and $R_s=0.115~\text{m}$, the advance ratio similarity,

$$J = \frac{U_{\infty}}{\Omega R} = \frac{V_{tunel}}{\Omega_{s} R_{s}}$$
 (2)

results in a $V_{tunnel} = 4.10 \text{ m/s}$ to satisfy the advance ratio similarity.

3. Results

Flow visualization: Particle Image Velocimetry (PIV) and smoke tests

Visualization results based on velocity contours around the building obtained with PIV tests in the wind tunnel, and building-helicopter smoke visualization tests will be presented in this section.

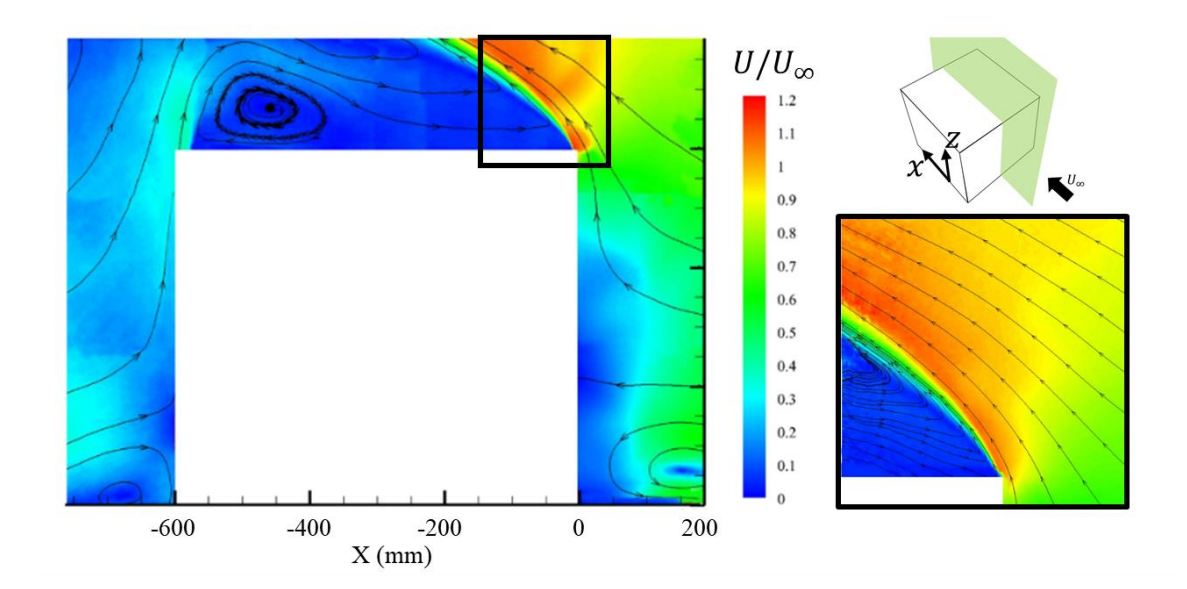


Fig. 6 PIV non-dimensional velocity contours around the building model.

Aerodynamics around the entire building is shown in the velocity contour of Figure 6 on the left. It can be observed that a recirculated region is formed in front of the building up to a height where a stagnation point is observed. In the upper part, the streamlines show the main flow detachment that starts on the upwind corner and the flow go upwards generating a big recirculation area above the roof. This flow may interfere with



the aircrafts on the rooftop heliport. A more detailed velocity contour of the flow at the edge of the building is shown in Figure 6 on the right.

To get a visual idea of how the aerodynamics of the building interfere with the helicopter, visualization studies using smoke with the scaled helicopter model operating at different points around the building are presented. Figure 7 shows photographs taken during tests, showing the aerodynamic interference at positions of the helicopter at 0.50 diameters (D) above the roof, and 0.65D to the rear wall and the side wall.

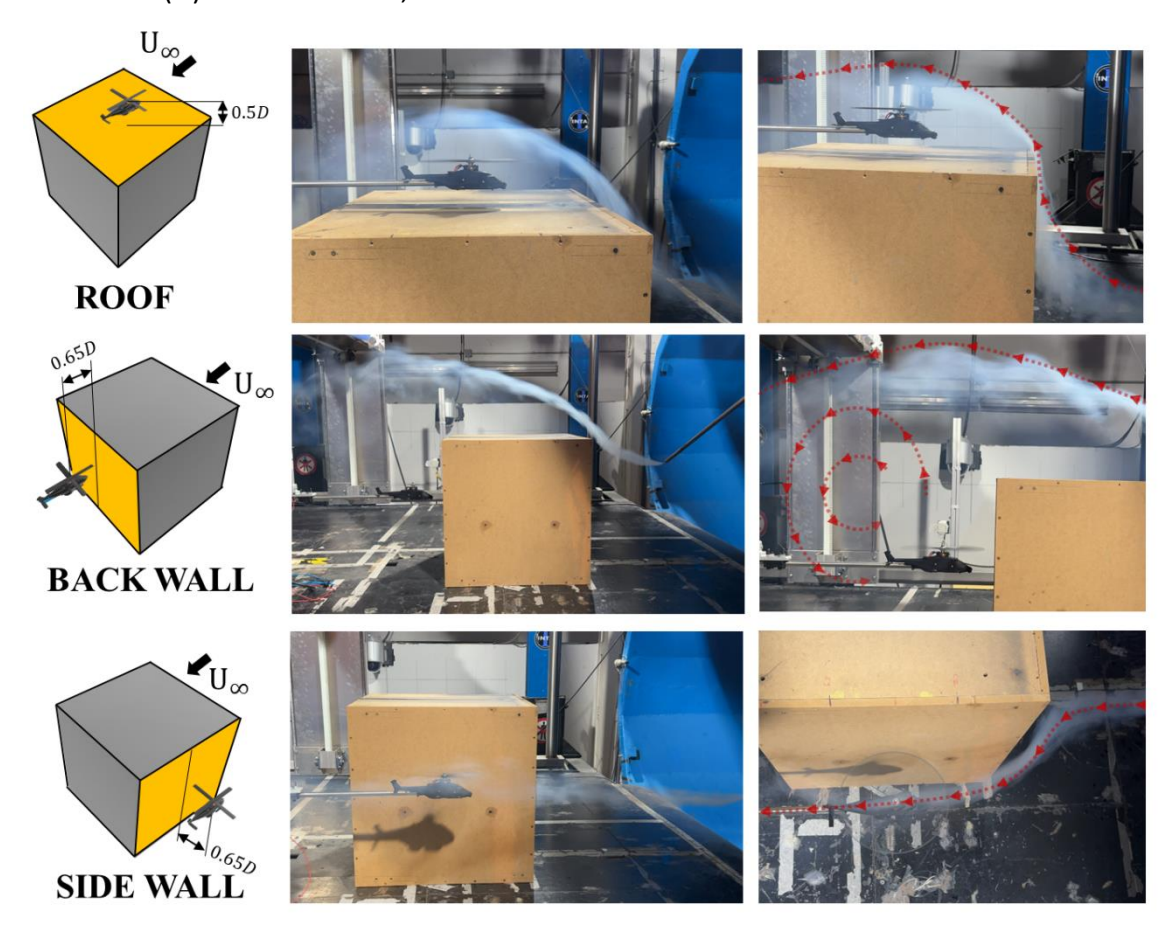


Fig. 7 Smoke visualization tests for building and helicopter aerodynamics interference.

When the helicopter is positioned on the roof, it is completely immersed in the detached area generated by the upwind corner. In addition, the edge of the shear region has been marked using a red dotted line. This shear layer appears to be at its maximum height in the center of the building (and the rotor), and is then reduced again, probably due to the effect of the flow absorbed during the main rotor operation.

The following case corresponds to the helicopter positioned on the rear wall. In this situation, the helicopter hovers in a completely detached region, generated by the detachment of the roof and side walls. Thus, the helicopter is in an area where there is low velocity recirculation, which has been represented by the red lines as seen in the

Florence 09 - 13 September 2024



frames of the video recorded during the visualization tests. The last case analyzed corresponds to the helicopter hovering close to the side wall. The flow deflected by the upwind corner of the sidewall bends and impacts directly against the helicopter rotor and fuselage.

Mean aerodynamic forces and moments

Using an automatic positioning system, the helicopter is placed in different points close the building walls and roof, with the helicopter always facing to the upcoming wind direction. Forces and moments are presented in non-dimensional terms as,

$$C_{Fi} = \frac{F_i}{\frac{1}{2}\rho(\Omega R)^2 S} \qquad C_{Mi} = \frac{M_i}{\frac{1}{2}\rho\Omega^2 R^3 S}$$
 (3)

where i=x,y,z corresponds to the different force and moments measured, ρ is the air density, Ω is the angular speed, R is the main helicopter rotor radius and S is the rotor surface.

In the first phase of tests, three helicopter positions with respect to the building were chosen, with the helicopter centered on the face of the building above the roof, on the rear wall and on the side wall. In each of them, the helicopter was positioned at different distances on the roof (between 0.35D and 2.00D), on the rear wall and on the side wall (0.65D-2.35D), with 0.05D differences between them. Figure 8 shows the results of the aerodynamic forces through vertical (C_{Fz}) and longitudinal (C_{Fx}) force coefficients acting on the helicopter in all the positions analysed. The helicopter distance to the roof or walls is plotted dimensioned with the rotor diameter (D) for each case.

In view of the results, when the helicopter is placed on the roof, positions lower than 1.00D of the rotor, translate into a significant variation of forces. Specifically, as the helicopter moves away from the roof, the forces increase by up to 80% in C_{FZ} , and then remain at a more or less constant value. For this reason, 0.50D is taken as the distance to be analyzed, as the helicopter is still deeply affected by the building aerodynamics.

The following case with the helicopter on the back wall shows effects of the building on the aerodynamic forces of the helicopter up to larger distances (1.75D). Especially the effects are observed on the longitudinal force coefficient (C_{Fx}) with fluctuations in the coefficient value of up to 66 %. The thrust coefficient is less affected in these cases, with maximum variations of less than 10%.

Finally, the case of the side wall, the aerodynamic coefficients also undergo significant variations up to distances of 2.00D. In fact, the longitudinal force (C_{Fx}) goes from practically zero near the wall (0.65D) to -5×10^{-3} (2.00D) when the building does not protect the helicopter from the wind. Thus, it is established that the distance to evaluate the effect of the building and its interaction with the helicopter aerodynamics on the lateral walls is analyzed at the minimum distance of 0.65D.



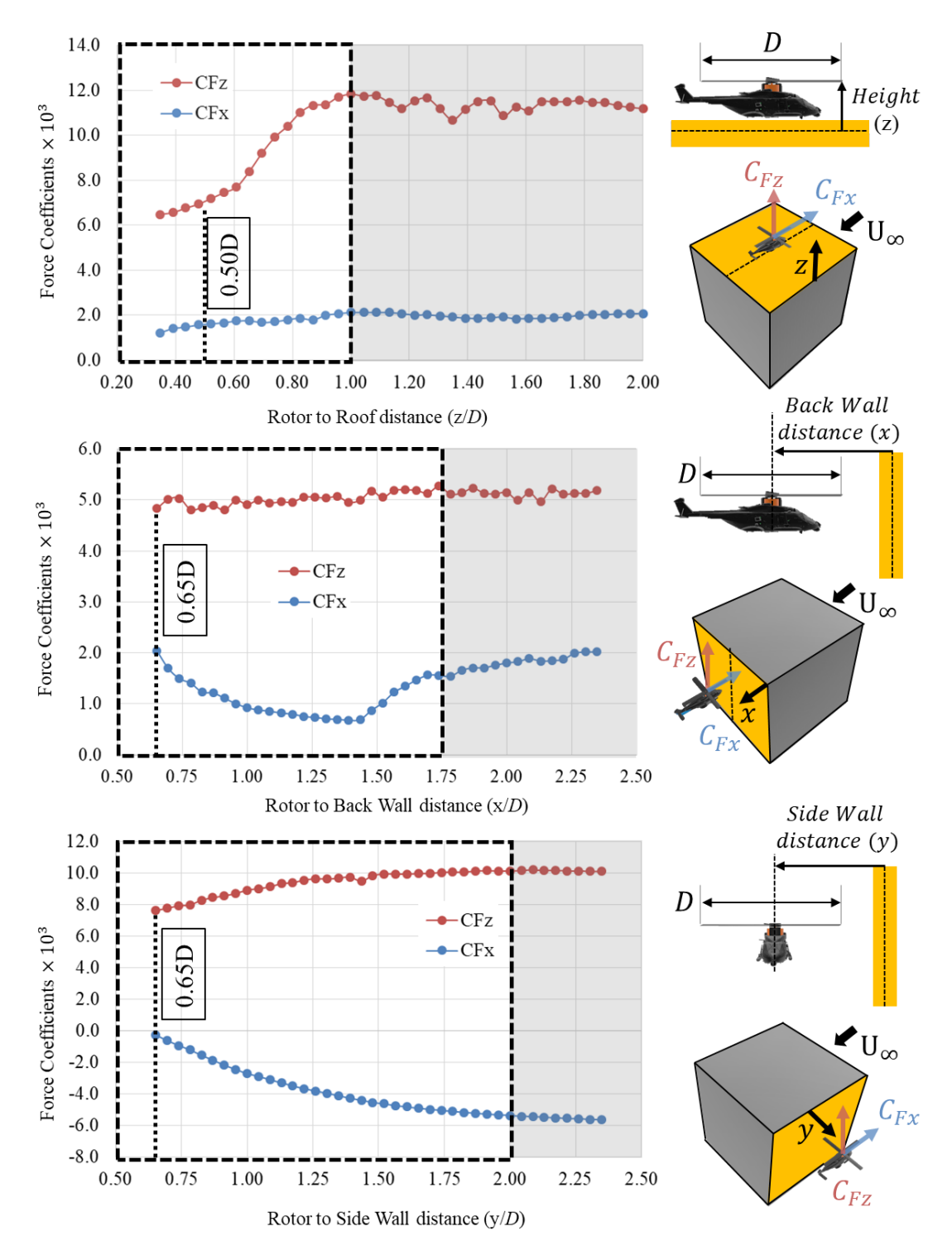


Fig. 8 Aerodynamic forces of the helicopter at different positions around the building.

Figures 9, 10 and 11 show the mean values (obtained from an average of 10 seconds acquisitions on each point analyzed) of the vertical or thrust force (C_{Fz}) , and the pitching (C_{My}) and rolling (C_{Mx}) moments at different points near the building. Above the roof at



distance 0.50D (figure 6), behind the rear wall at distance 0.65D (figure 7) and on the side wall at distance 0.65D (figure 8).

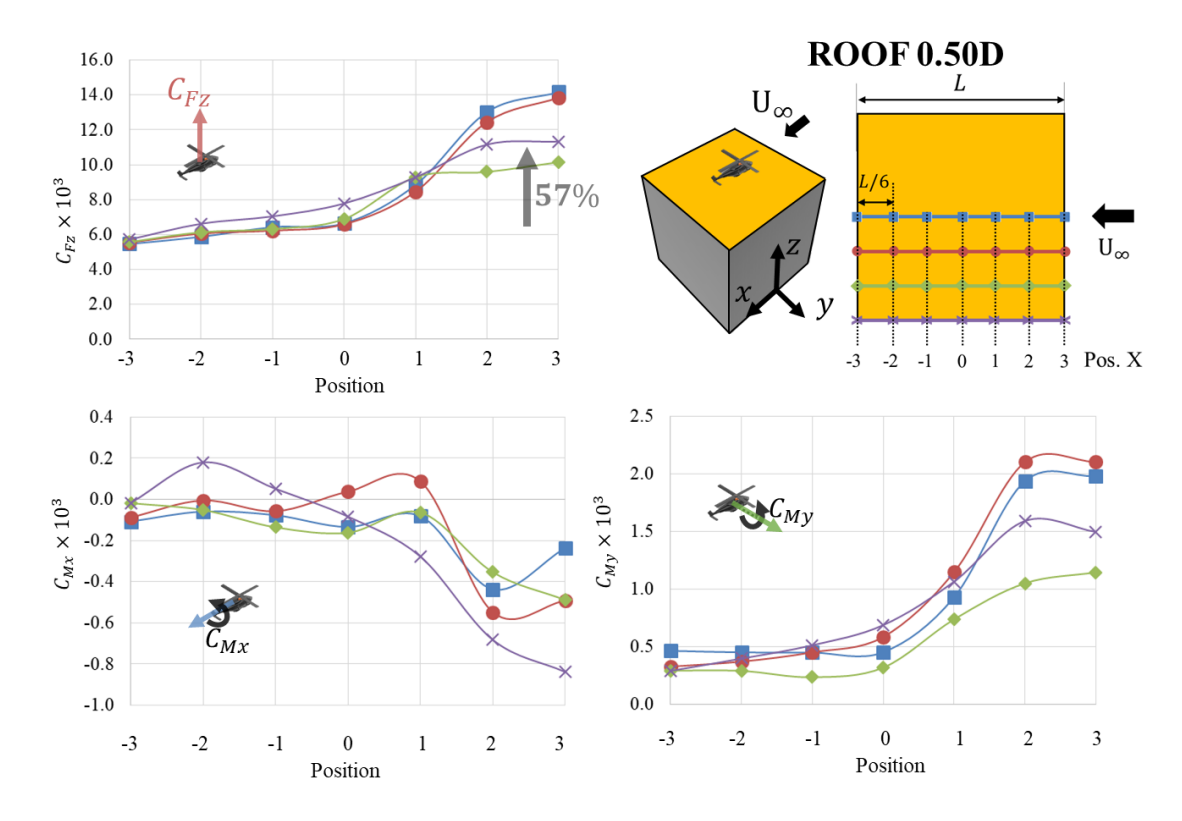


Fig. 9 Helicopter mean forces and moments at different positions above the roof (0.50D rotor height)

Starting with figure 9, the results are shown for 28 different positions above the roof. The positions over the center are shown using blue points, and the following positions closer to the side corner of the roof are in red, green and purple, respectively. The position of the helicopter with respect to the upwind corner is shown as a position on the X-axis, corresponding to -3 for the leeward corner, 0 for the central positions and +3 for the corner on which the wind is blowing (U_{∞}) . The step size between positions corresponds to a distance L/6, where L is the characteristic size of the building.

Thrust force coefficient (C_{FZ}) increases appreciably when the helicopter approaches the upwind corner (position 3). For example, in the cases where the helicopter is centered on the building (blue and red lines), it doubles its value, and when it is positioned towards the side corner (green and lilac lines) it suffers a smaller but significant increase of up to 57%. The pitching coefficient (C_{My}) follows the same trend, most likely caused by increased thrust, with constant values of $C_{My} = 0.4 \times 10^{-3}$, for all points at positions between -3 and 0, but with significant increases as the helicopter approaches the upwind corner (positions 0 to 3). Finally, the rolling coefficient (C_{Mx}) remains with a zero or very low values along positions -3 to 0, but again, when approaching the upwind side,



it changes to negative values. More importantly, the increase in C_{Mx} is greatest in the case closest to the side corner of the roof, with values of $C_{Mx} = -0.82 \times 10^{-3}$.

Figure 10 shows the results of aerodynamic forces and moments recorded at 36 positions at a distance of 0.65D on the rear wall. In this figure, the coefficients are shown at 9 different heights (from -2 to 6), which 6 are covered by the building (from -2 to 3), and 3 above the building roof (from 4 to 6).

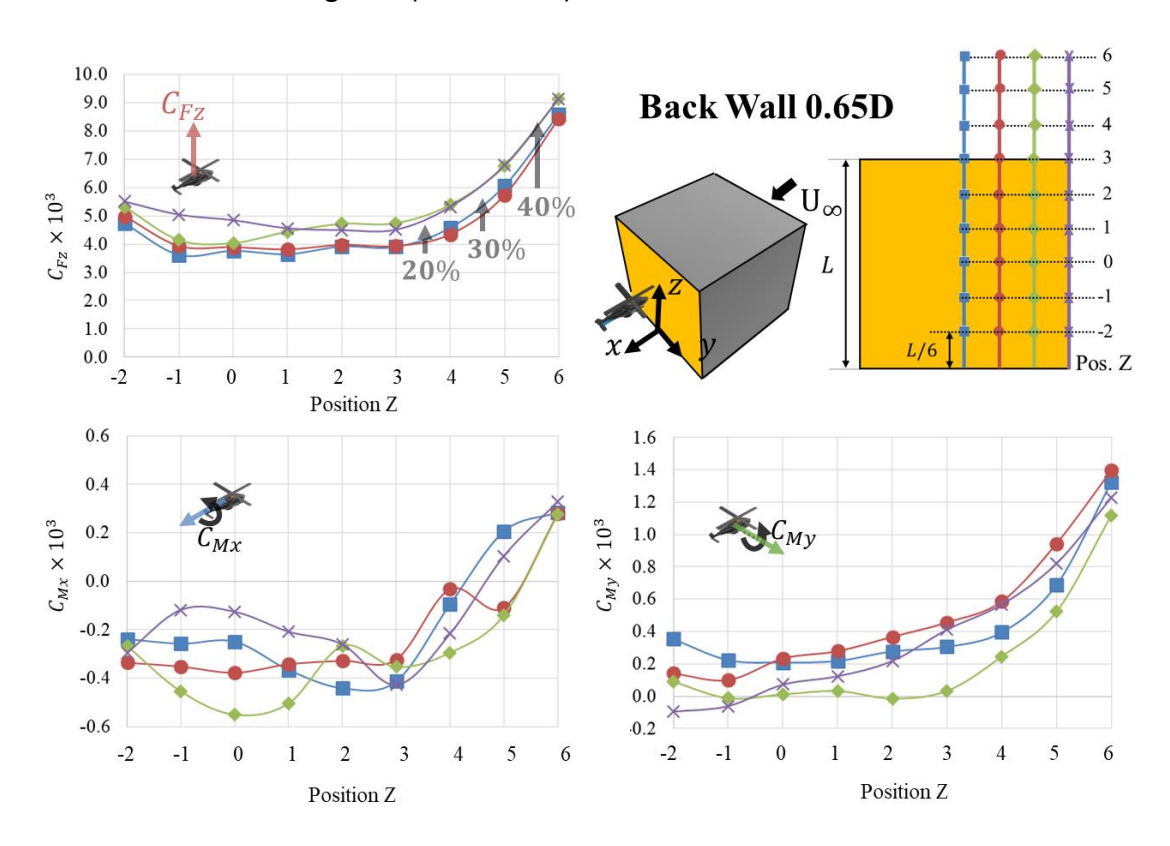


Fig. 10 Helicopter mean forces and moments at different positions above the roof (0.65D rotor distance)

When the helicopter is positioned behind the building, it is protected from the incidence of the wind, so the most relevant changes occur when the helicopter is above the height of the building. This effect is clearly observed in the thrust force (C_{Fz}) , with values for all cases around $C_{Fz} = 4 \times 10^{-3}$, but whose value increases by 20 % from position 3 to 4, 30 % from position 4 to 5, and 40 % from position 5 to 6. Similarly, the pitch and roll coefficients $(C_{My}$ and $C_{Mx})$ show that their values oscillate around 0 for the cases where the helicopter is covered by the building, but they increase significantly in positions 3 to 6. In particular, the pitch (C_{My}) is zero or slightly positive when the building aerodynamically covers the helicopter (positions -2 to 2), becoming clearly positive when the helicopter exceeds the height of the roof. The rolling moment (C_{Mx}) is zero or slightly negative at low positions (-2 to 2) but becomes positive due to the effect of the wind on the roof. This implies that if an ascent is made along the rear wall, the helicopter may be immersed in flow instabilities generated by the building over the roof.



Figure 11 shows the results obtained with the helicopter operating on the side wall of the building at a distance of 0.65D to the center of the rotor. Since the problem on the side is not symmetrical, a larger number of points (63 points) were recorded. In this case, the helicopter is not covered by the building and all points are directly affected by the incident wind. As a result, there are not as large fluctuations from one position to another as in the previous case.

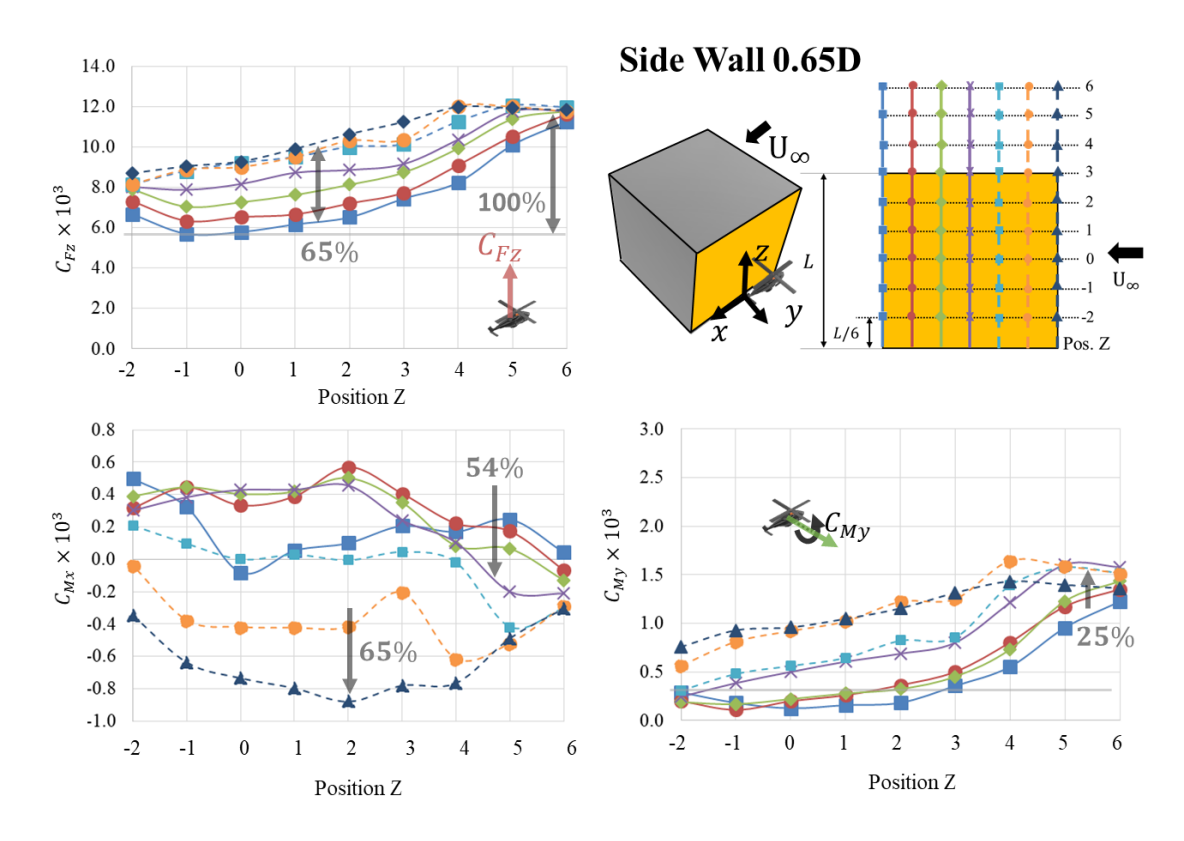


Fig. 11 Helicopter mean forces and moments at different positions above the roof (at 0.65D rotor distance)

In the case of the thrust coefficient (C_{Fz}), it is observed that as the helicopter moves to a higher altitude (position Z), there is an increase in the coefficient. This increase is smooth for almost all cases between positions -1 and 2. However, as the helicopter approaches and overpass the roof (positions 3 to 6), the increase is more pronounced. Another observable trend is that as the helicopter is positioned closer to the upwind corner, the thrust coefficient also becomes larger, being minimum at the positions downstream of the incident wind (light blue squares) and maximum at the corner positions (dark blue triangles). In conclusion, different helicopter positions at the same height cause differences in helicopter traction of up to 65%. And different helicopter heights can cause changes in traction of up to 100%, for example, doubling values from position 0 to position 6. Note also that at position 6 all cases show an equivalent thrust value, since the helicopter is outside the aerodynamic influence of the building.

Florence 09 - 13 September 2024



Regarding the pitching moment (C_{My}), there is a similar tendency as in the case of thrust. Its values are around 0 for low altitude positions (between -2 and 2) only if the helicopter is close to the downwind corner of the building (light blue, red and green curves). In all cases, higher positions (3 to 6) indicate a clear increase in the value of the pitch coefficient, tripling the value for downstream positions and increasing by up to 25 % for positions in the upwind corner with respect to the downstream corner of the flow. Finally, several trends are observed in the rolling coefficient (C_{Mx}). All the curves at positions near the downwind corner (blue, red, green and purple) show slightly positive values of balance, indicating a tendency for the helicopter to rotate towards the wall. However, as positions approach the upwind corner (light blue, yellow and dark blue curves), C_{Mx} is negative causing the helicopter to have a tendency to move away from the wall. In general, the reductions in C_{Mx} as height increases are up to 54% for cases of the helicopter in downstream positions, and up to a 65% increase for cases near the upwind corner.

4. Conclusions

The combination of building and helicopter aerodynamics are in the spotlight since the concept of Urban Air Mobility (UAM) has received wider attention in the last years. Operate aircraft around buildings involve challenges because the aerodynamic flows they face are complex, non-stationary and turbulent. Wind tunnel studies that combine buildings and aircraft could provide the necessary information to fully understand the problem. In this study, wind tunnel tests with scaled models of a simple building and a NH Industries NH90 helicopter have been performed. The Particle Image Velocimetry (PIV) and smoke visualization tests have been used to introduce the aerodynamic problem. Later, as the helicopter is equipped with an internal balance, the mean aerodynamic forces and moments measured have been analyzed with the helicopter hovering at different points around the building.

The conclusions extracted from visualization tests are:

- ➤ PIV visualization around the building displayed an important flow detachment on the upwind corner and a huge recirculation region above the building roof that may interfere with the aircrafts on the rooftop heliport.
- Smoke visualization tests showed that when the helicopter is positioned on the roof, it is completely immersed in the detached area generated by the upwind corner, and the shear layer is curved due to the effect of the main rotor operation. The helicopter placed next to the rear wall reveals that the operation is performed inside a low velocity and recirculation flow behind the building. And the deflected flow by the frontal face of the building impacts directly to the aircraft that hovers close to the lateral wall.

Florence 09 - 13 September 2024



The results with the helicopter centered above the roof, back and side walls, and at different heights revealed that above the roof, significant variations in aerodynamic forces for positions closer than 1.00D. On the rear wall, longitudinal force coefficient experiences fluctuations of up to 66%, and thrust coefficient of less than 10%, and the distance for significant aerodynamic effect for the helicopter is determined to be 0.65D from the wall. Finally, on the side wall, the aerodynamic coefficients vary significantly up to a distance of 2.00D from the wall. And the distance selected to assess the building's aerodynamic impact on the helicopter was established again at 0.65D.

The conclusions obtained from the mean forces and moments of helicopter can be summarized as follows:

- \triangleright 0.50D above the roof: Thrust force (C_{Fz}) increases notably when the helicopter approaches the upwind corner, doubling the value when the helicopter is centered on the building, and increasing a 57% when it is positioned towards the side corner. The pitching coefficient (C_{My}) follows the same trend, and the rolling coefficient (C_{Mx}) change to negative values as the helicopter approach the upwind side.
- \blacktriangleright 0.65D to the rear wall: when the helicopter is covered by the building, smooth changes are experienced. Relevant changes occur when the helicopter is above the height of the building. Thrust force (C_{FZ}), increases by 20 %, 30% and 40% between different positions in height. Pitch and roll coefficients (C_{My} and C_{Mx}) show null values when the helicopter is covered by the building, but they increase significantly with the height. This implies that if an ascent is made along the rear wall, the helicopter may be immersed in flow instabilities generated by the building over the roof.
- \triangleright 0.65D to the side wall: Thrust coefficient (C_{Fz}) magnifies as the helicopter moves to a higher altitude and closer to the upwind corner. Different helicopter positions at the same height cause differences in helicopter thrust of up to 65%., but different helicopter heights can cause changes up to 100%. Pitching moment (C_{My}) behavior is similar to the thrust. Its values are null for low altitude, tripling the value for downstream positions and increasing by up to 25 % for positions in the upwind corner with respect to the downstream corner of the flow. Rolling coefficient (C_{Mx}) revealed a tendency for the helicopter to rotate towards the wall, and a contrary tendency when it approaches the upwind corner.

This kind of studies should be carried out in wind tunnels using detailed models of buildings to ensure safety for helicopters during emergency operations in the vicinity of buildings, or to ensure the operational safety for future aircraft operating in cities.

Florence 09 – 13 September 2024



Copyright Statement

The authors confirm that they, and/or their company or organization, hold copyright on all of the original material included in this paper. The authors also confirm that they have obtained permission, from the copyright holder of any third party material included in this paper, to publish it as part of their paper. The authors confirm that they give permission, or have obtained permission from the copyright holder of this paper, for the publication and distribution of this paper as part of the ICAS proceedings or as individual off-prints from the proceedings.

References

- [1] Łusiak, T. & Dziubinski, A., Szumański, K. "Interference between helicopter and its surroundings, experimental and numerical analysis". *Task Quarterly*. 13, 2009.
- [2] Rowe S. J. "The response of helicopters to aerodynamic disturbances around offshore helidecks" *RAeS Conf. on Helicopter Operations in the Maritime Environment*. London, UK, 2001.
- [3] C. H., Wang, Y., White, M. D., and Owen, I., "An experimental technique for evaluating the aerodynamic impact of ship superstructures on helicopter operations," *Ocean Engineering*, vol. 61, 2013, pp. 97–108. doi: 10.1016/j.oceaneng.2012.12.052
- [4] Bardera-Mora, R., León Calero, M., and García-Magariño, A., "Aerodynamic effect of the aircraft carrier island on flight deck flow with Cross Wind," *Proceedings of the Institution of Mechanical Engineers*, Part M: Journal of Engineering for the Maritime Environment, vol. 232, 2017, pp. 145–154. doi: 10.1177/1475090216689172
- [5] Healey, J. Val., "Establishing a database for flight in the wakes of structures," *Journal of Aircraft*, vol. 29, 1992, pp. 559–564.
- [6] Dooley, G. M., Krebill, A. F., Martin, J. E., Buchholz, J. H. J., and Carrica, P. M., "Structure of a Ship Airwake at Multiple Scales," *AIAA Journal*, Vol. 58, No. 5, 2020, pp. 2005–2013. doi: 10.2514/1.J058994
- [7] Thedin, R., Murman, S., Horn, J., and Schmitz, S., "Effects of Atmospheric Turbulence Unsteadiness on Ship Airwakes and Helicopter Dynamics," *Journal of Aircraft*, Vol. 57, No. 3, 2020, pp. 534–546. doi: 10.2514/1.C035643
- [8] Yuan, W., Wall, A., & Lee, R. (2018). "Combined numerical and experimental simulations of unsteady ship airwakes". *Computers & Fluids*, 172, 29-53.
- [9] Crozon, C., Steijl, R., and Barakos, G. N., "Numerical Study of Helicopter Rotors in a Ship Airwake," *Journal of Aircraft*, Vol. 51, No. 6, 2014, pp. 1813–1832. doi: 10.2514/1.C032535

Florence 09 - 13 September 2024



- [10] Brownell, C., L. Luznik, M. Snyder, H. Kang and C. Wilkinson. 2012. "In Situ Velocity Measurements in the Near-Wake of a Ship Superstructure". *Journal of Aircraft*. 49(5):1440-1450.
- [11] Bardera, R., "Flow field velocity on the flight deck of a frigate," *Proceedings of the Institution of Mechanical Engineers, Part G: Journal of Aerospace Engineering*, vol. 228, 2014, pp. 2674–2680.
- [12] Bardera-Mora, R., Barcala-Montejano, M., Rodríguez-Sevillano, A., de Diego, G., & de Sotto, M. (2015). "A spectral analysis of laser Doppler anemometry turbulent flow measurements in a ship air wake". *Proceedings Of The Institution Of Mechanical Engineers, Part G: Journal Of Aerospace Engineering*, 229(12), 2309-2320.
- [13] Van Muijden, J., Boelens, O., van der Vorst, J., and Gooden, J., "Computational Ship Airwake Determination to Support Helicopter-Ship Dynamic Interface Assessment," *21st AIAA Computational Fluid Dynamics Conference*, AIAA Paper 2013-3078, 2013. doi: 10.2514/6.2013-3078
- [14] Wakefield, N. H., Newman, S. J., and Wilson, P. A., "Helicopter Flight Around a Ship's Superstructure," *Proceedings of the Institution of Mechanical Engineers, Part G: Journal of Aerospace Engineering*, Vol. 216, No. 1, 2002, pp. 13–28. <u>doi: 10.1243/0954410021533391</u>
- [15] Lee, R. and S. Zan. 2005. Wind Tunnel Testing of a Helicopter Fuselage and Rotor in a Ship Airwake. *Journal of the American Helicopter Society*. 50(4):326-337.
- [16] Wadcock, A. J., G. K. Yamauchi, J. T. Heineck, M. J. Silva and K. R. Long. "PIV Measurements of the Wake of a Tandem-Rotor Helicopter in Proximity to a Ship". *National Aeronautics and space administration* moffett field CA AMES research center. 2004
- [17] Doane, S. R. and D.A. Landman. 2012. "A wind tunnel investigation of ship airwake/rotor downwash coupling using design of experiments methologies". In: Proceedings of the 50th AIAA Aerospace Sciences Meeting including the New Horizons Forum and Aerospace Exposition. 2012-0767.
- [18] Silva, Mark J. Yamauchi, Gloria K. Wadcock, Alan J. Long, Kurtis R., "Wind tunnel investigation of the aerodynamic interactions between helicopter and tilt-rotors in a shipboard environment". *American Helicopter Society 4th Decennial Specialist's Conf. on Aeromechanics*, San Francisco, CA, 2004.
- [19] Derby, M., and Yamauchi, G., "Design of 1/48th-scale models for ship/rotorcraft interaction studies," *21st AIAA Applied Aerodynamics Conference*, 2003. doi: 10.2514/6.2003-3952
- [20] Wang, Y., Curran, J., Padfield, G. D., and Owen, I., "AirDyn: An instrumented model-scale helicopter for measuring unsteady aerodynamic loading in airwakes,"

Florence 09 - 13 September 2024



Measurement Science and Technology, vol. 22, 2011, p. 045901. doi: 10.1088/0957-0233/22/4/045901

- [21] Kääriä, C. H., Forrest, J. S., and Owen, I., "The virtual airdyn: A simulation technique for evaluating the aerodynamic impact of ship superstructures on helicopter operations," *The Aeronautical Journal*, vol. 117, 2013, pp. 1233–1248. doi: 10.1017/s0001924000008836
- [22] Taymourtash, N., Zanotti, A. Gilbertini, G. Quaranta, G. "Simulation and Testing of Helicopter-ship Aerodynamic Interaction". *47th European Rotorcraft Forum*, Glasgow, Scotland, 7-9 September, 2021.
- [23] 2005 ASHRAE handbook Fundamentals. (2005). 1st ed. Atlanta, GA.: ASHRAE, Chapter 16: Airflow Aroud Buildings.
- [24] Handbook, A. S. H. R. A. E. (2005). Fundamentals (SI Edition), ASHRAE Inc. *Atlanta*, 31-47.
- [25] Jinsheng Cai, Her-Mann Tsai, Shijun Luo and Feng Liu. "Vortex Core and Its Effects on the Stability of Vortex Flow over Slender Conical Bodies". Unevirsity of California, Irivine, CA.
- [26] D. Banks and R. N. Meroney. "A model of roof-top surfaces pressures produced by conical vortices: Evaluation and implications". Colorado State University, Fort Collins U.S.A.
- [27] Franchini, S., Pindado, S., Meseguer, J. and Sanz-Andrés, A. (2005). "A parametric, experimental analysis of conical vortices on curved roofs of low-rise buildings". Journal of Wind Engineering and Industrial Aerodynamics, 93(8), pp.639-650.
- [28] Lewe, J.-H. et al. "An integrated decision-making method to identify design requirements through agent-based simulation for personal air vehicle system." AIAA's Aircraft Technology, Integration, and Operations (ATIO) 2002 Technical Forum. 2002.
- [29] McKinley, J. B. "Evaluating Wind Flow Around Buildings on Heliport Placement." *Defense Technical Information Center*, 1984, ADA-A153 512, DOT/FAA/PM-84/25, https://apps.dtic.mil/dtic/tr/fulltext/u2/a153512.pdf.
- [30] Fadhil, D. N. "A GIS-Based Analysis for Selecting Ground Infrastructure Locations for Urban Air Mobility." *inlangen*]. *Master's Thesis, Technical University of Munich*, 2018.
- [31] 1Lee, R. G., and Zan, S. J., "Unsteady aerodynamic loading on a helicopter fuselage in a ship Airwake," *Journal of the American Helicopter Society*, vol. 49, 2004, pp. 149–159. doi: 10.4050/jahs.49.149
- [32] Thedin, R., Kinzel, M. P., Horn, J. F., and Schmitz, S., "Coupled Simulations of Atmospheric Turbulence-Modified Ship Airwakes and Helicopter Flight Dynamics," *Journal of Aircraft*, Vol. 56, No. 2, 2019, pp. 812–824. doi: 10.2514/1.C035158

Florence 09 – 13 September 2024



- [33] Memon, W. A., Owen, I., and White, M. D., "Motion Fidelity Requirements for Helicopter-Ship Operations in Maritime Rotorcraft Flight Simulators," *Journal of Aircraft*, Vol. 56, No. 6, 2019, pp. 2189–2209. doi: 10.2514/1.C035521
- [34] Watson, N. A., Owen, I., and White, M. D., "Piloted Flight Simulation of Helicopter Recovery to the Queen Elizabeth Class Aircraft Carrier," *Journal of Aircraft*, Vol. 57, No. 4, 2020, pp. 742–760. doi: 10.2514/1.C035733
- [35] Forrest, J., Kaaria, C., and Owen, I., "Evaluating Ship Superstructure Aerodynamics for Maritime Helicopter Operations Through CFD and Flight Simulation," *Aeronautical Journal*, Vol. 120, No. 1232, 2016, pp. 1578–1603. doi: 10.1017/aer.2016.76
- [36] Forsythe, J., Lynch, E., Polsky, S., and Spalart, P., "Coupled Flight Simulator and CFD Calculations of Ship Airwake Using Kestrel," *53rd AIAA Aerospace Sciences Meeting*, AIAA Paper 2015-0556, 2015. doi: 10.2514/6.2015-0556
- [37] Foeken, M. Pavel, M. D. "Investigation on the simulation of helicopter/ship operations". *Faculty of Aerospace Engineering*, Delft University of Technology Kluyverweg 1, 2629 HS, Delft, The Netherlands.
- [38] Mehling, T., Halbe, O., Gasparac, T., Vrdoljak, M., and Hajek, M. "Piloted Simulation of Helicopter Shipboard Recovery with Visual and Control Augmentation". *In AIAA Scitech 2021 Forum*. 2021. doi: 10.2514/6.2021-1136
- [39] Raffel, M., Willert, C. E., Scarano, F., Kähler, C. J., Wereley, S. T., and Kompenhans, J., Particle image velocimetry: A practical guide, Cham: Springer International Publishing, 2018.
- [40] Adrian, R. J., and Westerweel, J., Particle image velocimetry, Cambridge: Cambridge University Press, 2011.
- [41] Prasad, A. K. "Particle image velocimetry". Current science-bangalore, 79(1), 51-60, 2000.
- [42] Adrian, R. J., "Particle-imaging techniques for Experimental Fluid Mechanics," Annual Review of Fluid Mechanics, vol. 23, 1991, pp. 261–304. doi: 10.1146/annurev.fl.23.010191.001401
- [43] Simiu, E., and Scanlan, R. H. "Wind effects on structures: fundamentals and applications to design." John Wiley &Sons, INC, 1996.